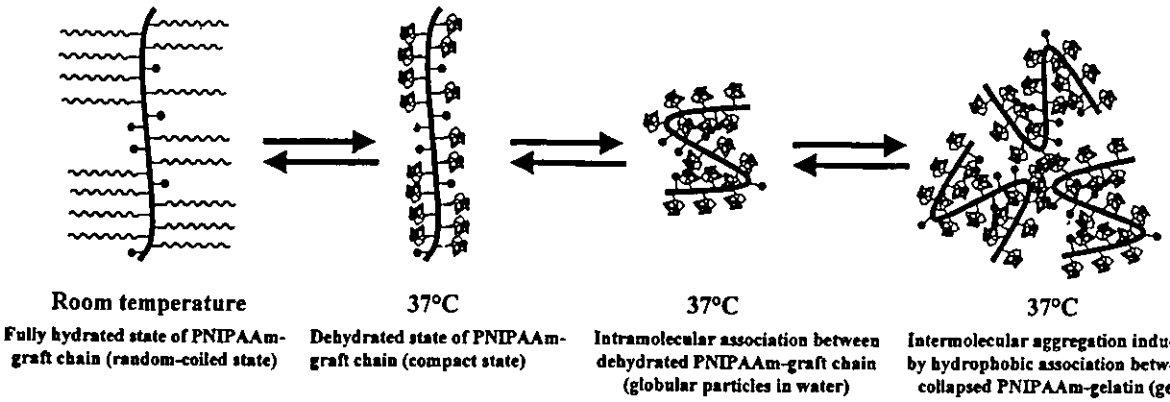

SCHEME 2. Schematic of mechanism of PNIPAAm-gelatin gelation.

chanical properties of tissue-engineered cartilages approach those of native hyaline cartilage as the culture period proceeds.

Cell viability strongly depended on the concentration of PNIPAAm-gelatin and molecular weight of the PNIPAAm graft chain (Fig. 2). Few cells died in the gel prepared at low concentration (5%) of PNIPAAm-gelatin with high molecular weight PNIPAAm graft chains (1.3×10^5 g/mol), which was verified by both DNA counting and a living cell/dead cell staining technique using CLSM. This may be explained as follows. The increase in PNIPAAm graft chain length should enhance the intermolecular aggregation of collapsed PNIPAAm chains, resulting in a higher degree of aggregation state than that of the lower molecular weight PNIPAAm graft chain. In addition, theoretically a lower PNIPAAm-gelatin concentration produces a higher void in the gel. The combination of a high molecular weight graft chain and low PNIPAAm-gelatin concentration could produce a large open cell-structured gel with highly localized and densely aggregated PNIPAAm-gelatin molecules and large voids, which eventually facilitate diffusion of oxygen and nutrients and provide large ample space for cell entrapment without excessive interaction of the cell membrane with PNIPAAm-gelatin or gelation-induced mechanical deformation of cells, both of which impair cells. (Note that such graft architecture- and concentration-dependent cell viability/death characteristics were first observed for smooth muscle cells [unpublished data]).

Chondrogenesis of the incorporated cells in the tissue-engineered cartilage occurred with culture time, which is concluded from the following experimental results: (1) there was no sign of either cell death or proliferation in the gel prepared from the appropriate PNIPAAm-gelatin (Gel A) during 3 weeks of culture; (2) the population of cells with round-shaped morphology, which is characteristic of chondrocytes in normal native tissue, rapidly increased as the culture period proceeded; (3) flow cytometric analysis showed that most of the cells had entered the G_0/G_1 phase even at 1 week of culture, at which time approximately 90% of cells were in the G_0/G_1 phase. These results indicate that dedifferentiated cells (or proliferative cells) were phenotypically transformed to redifferentiated cells in the tissue-engineered cartilage as in the normal cartilage; and (4) the amount of deposits of type II collagen and s-GAG in the tissue-engineered cartilage increased with culture time (Figs. 6 and 7), but little deposit of type I collagen was noted (Fig. 6). Although type II collagen and s-GAG are specific markers for the differentiated phenotype characteristic, type I collagen is a specific marker for dedifferentiated phenotype.[30] Taken together, all of the results strongly indicate that the use of PNIPAAm-gelatin scaffolds enables the induction and maintenance of cell redifferentiation.

It is of interest to note that a 12 week-cultured tissue-engineered cartilage, which has an opaque appearance at 37°C, did not shrink, in contrast to collagen-based tissue-engineered cartilage. The tissue-engineered cartilage that was left to stand at room temperature did not dissolve and was semitransparent, resembling native hyaline cartilage. These results suggest that the long term-cultured tissue-engineered cartilage was filled with specific ECMs of hyaline cartilage, contributing to its structural integrity, and that PNIPAAm-gelatin was not yet degraded in such an *in vitro* environment.

The maximum strain that results mainly from collagen synthesis tended to decrease with culture time, and the residual strain that results mainly from s-GAG synthesis markedly decreased over the entire 8 weeks of culture. No further decrease was observed beyond this period. Both mechanical properties tended to approach those of rabbit articular cartilage with culture time, although these values were still higher than those of native cartilage. These results suggest that remodeling of tissue architecture was not yet completed in terms of macromolecular assemblies and orientation as well as amount. Since tissue-engineered cartilages was cultured in a static envi-

ronment, orientation of ECMs in the direction of mechanical stress in tissue-engineered cartilage is not expected.

Our ongoing study is focused on *in vivo* tissue-engineered cartilage remodeling and spatio- and temporomorphogenesis on *in situ* gelation using PNIPAAm-gelatin and *in vitro* tissue remodeling of tissue-engineered cartilages subjected to periodically loaded compression stress.

ACKNOWLEDGMENTS

We thank Shoji Ohya for the method for synthesis of PNIPAAm–gelatin and Yumiko Miura for her contribution to preparation of laboratory materials. This study was financially supported by the Promotion Fundamental Studies in Health Science of the Organization for Pharmaceutical Safety and Research (OPSR) under grant 97-15, and in part by a Grant-in-Aid for Scientific Research (A2-12358017, B2-12470277) from the Ministry of Education, Culture, Sports, Science, and Technology of Japan.

REFERENCES

1. Buckwalter, J.A., and Mankin, H.J. Articular cartilage: Tissue design and chondrocyte–matrix interactions. Instr. Course Lect. **47,** 477, 1998.
2. Buckwalter, J.A. Articular cartilage: Injuries and potential for healing. J. Orthop. Sports Phys. Ther. **28,** 192, 1998.
3. Kim, H.K., Moran, M.E., and Salter, R.B. The potential for regeneration of articular cartilage in defects created by chondral shaving and subchondral abrasion: An experimental investigation in rabbits. J. Bone Joint Surg. Am. **73,** 1301, 1991.
4. Johnson, L.L. Arthroscopic abrasion arthroplasty in historical and pathologic perspective: Present status. Arthroscopy **2,** 54, 1986.
5. Insall, J. The Pridie debridement operation for osteoarthritis of the knee. Clin. Orthop. **101,** 61, 1974.
6. Mitchell, N., and Shepard, N. The resurfacing of adult rabbit articular cartilage by multiple perforations through the subchondral bone. J. Bone Joint Surg. Am. **58,** 230, 1976.
7. Hangody, L., Kish, G., Karpati, Z., Udvarhelyi, I., Szigeti, I., and Bely, M. Mosaicplasty for the treatment of articular cartilage defects: Application in clinical practice. Orthopedics **21,** 751, 1998.
8. Brittberg, M., Lindahl, A., Nilsson, A., Ohlsson, C., Isaksson, O., and Peterson, L. Treatment of deep cartilage defects in the knee with autologous chondrocyte transplantation. N. Engl. J. Med. **331,** 889, 1994.
9. Wakitani, S., Imoto, K., Yamamoto, T., Saito, M., Murata, N., and Yoneda, M. Human autologous culture expanded bone marrow mesenchymal cell transplantation for repair of cartilage defects in osteoarthritic knees. Osteoarthritis Cartilage **10,** 199, 2002.
10. Homminga, G.N., Buma, P., Koot, H.W., van der Kraan, P.M., and van den Berg, W.B. Chondrocyte behavior in fibrin glue in vitro. Acta Orthop. Scand. **64,** 441, 1993.
11. Guo, J.F., Jourdian, G.W., and MacCallum, D.K. Culture and growth characteristics of chondrocytes encapsulated in alginate beads. Connect. Tissue Res. **19,** 277, 1989.
12. Elisseeff, J., Anseth, K., Sims, D., McIntosh, W., Randolph, M., Yaremchuk, M., and Langer, R. Transdermal photopolymerization of poly(ethylene oxide)-based injectable hydrogels for tissue-engineered cartilage. Plast. Reconstr. Surg. **104,** 1014, 1999.
13. Elisseeff, J., McIntosh, W., Anseth, K., Riley, S., Ragan, P., and Langer, R. Photoencapsulation of chondrocytes in poly(ethylene oxide)-based semi-interpenetrating networks. J. Biomed. Mater. Res. **51,** 164, 2000.
14. Cao, Y., Rodriguez, A., Vacanti, M., Ibarra, C., Arevalo, C., and Vacanti, C.A. Comparative study of the use of poly(glycolic acid), calcium alginate and pluronics in the engineering of autologous porcine cartilage. J. Biomater. Sci. Polym. Ed. **9,** 475, 1998.
15. Saim, A.B., Cao, Y., Weng, Y., Chang, C.N., Vacanti, M.A., Vacanti, C.A., and Eavey, R.D. Engineering autogenous cartilage in the shape of a helix using an injectable hydrogel scaffold. Laryngoscope **110,** 1694, 2000.
16. Morikawa, N., and Matsuda, T. Thermoresponsive artificial extracellular matrix: *N*-Isopropylacrylamide-graft-copolymerized gelatin. J. Biomater. Sci. Polymer Edn. **13,** 167, 2002.
17. Matsuda, T. Molecular design of functional artificial extracellular matrix. Jpn. J. Artif. Organs **28,** 242, 1999.
18. Ohya, S., Nakayama, Y., and Matsuda, T. Material design for artificial extracellular matrix: Cell entrapment in poly(*N*-isopropylacrylamide) (PNIPAM) grafted gelatin hydrogel. J. Artif. Organs **4,** 308, 2001.
19. Heskins, M., and Guillet, J.E. Solution properties of poly(*N*-isopropylacrylamide). J. Makromol. Sci. Chem. **A2,** 1441, 1968.
20. Yasui, N., Osawa, S., Ochi, T., Nakashima, H., and Ono, K. Primary culture of chondrocytes embedded in collagen gels. Exp. Cell Biol. **50,** 92, 1982.
21. Beier, F., Leask, T.A., Haque, S., Chow, C., Taylor, A.C., Lee, R.J., Pestell, R.G., Ballock, R.T., and LuValle, P. Cell cycle genes in chondrocyte proliferation and differentiation. Matrix Biol. **18,** 109, 1999.
22. Kumagai, J., Sarkar, K., Uhthoff, H.K., Okawara, Y., and Ooshima, A. Immunohistochemical distribution of type I, II, and III collagens in the rabbit supraspinatus tendon insertion. J. Anat. **185,** 279, 1994.
23. Miller, E.J., and Rhodes, R.K. Preparation and characterization of the different types of collagen. Methods Enzymol. **82,** 33, 1982.
24. Otsu, T., Yoshida, M., and Tazaki, T. A model of for living radical polymerization. Macromol. Chem. Rapid Commun. **3,** 133, 1982.
25. Brittberg, M., Nilsson, A., Lindahl, A., Ohlsson, C., and Peterson, L. Rabbit articular cartilage defects treated with autologous cultured chondrocytes. Clin. Orthop. **326,** 270, 1996.
26. Freed, L.E., Marquis, J.C., Nohria, A., Emmanual, J., Mikos, A.G., and Langer, R. Neocartilage formation in vitro

and in vivo using cells cultured on synthetic biodegradable polymers. J. Biomed. Mater. Res. **27,** 11, 1993.
27. Rahfoth, B., Weisser, J., Sternkopf, F., Aigner, T., von der Mark, K., and Brauer, R. Transplantation of allograft chondrocytes embedded in agarose gel into cartilage defects of rabbits. Osteoarthritis Cartilage **6,** 50, 1998.
28. Kawamura, S., Wakitani, S., Kimura, T., and Maeda, A., Caplan, A.I., Shino, K., and Ochi, T. Articular cartilage repair: Rabbit experiments with a collagen gel-biomatrix and chondrocytes cultured in it. Acta Orthop. Scand. **69,** 56, 1998.
29. Katsube, K., Ochi, M., Uchio, Y., Maniwa, S., Matsusaki, M., Tobita, M., and Iwasa, J. Repair of articular cartilage defects with cultured chondrocytes in Atelocollagen gel: Comparison with cultured chondrocytes in suspension. Arch. Orthop. Trauma Surg. **120,** 121, 2000.
30. Mayne, R., Vail, M.S., Mayne, P.M., and Miller, E.J. Changes in type of collagen synthesized as clones of chick chondrocytes grow and eventually lose division capacity. Proc. Natl. Acad. Sci. U.S.A. **73,** 1674, 1976.

Address reprint requests to:
Takehisa Matsuda, Ph.D.
Department of Biomedical Engineering
Graduate School of Medicine, Kyushu University
3-1-1 Maidashi, Higashi-ku,
Fukuoka 812-8582
Japan

E-mail: matsuda@med.kyushu-u.ac.jp

Coaxial double-tubular compliant arterial graft prosthesis: time-dependent morphogenesis and compliance changes after implantation

Hiromichi Sonoda,[1,2,3] Keiichi Takamizawa,[1] Yasuhide Nakayama,[1] Hisataka Yasui,[2] Takehisa Matsuda[3]
[1]*Department of Biomedical Engineering, National Cardiovascular Center Research Institute, 5-7-1 Fujishirodai, Suita, Osaka 565-8565, Japan*
[2]*Department of Cardiovascular Surgery, Graduate School of Medicine, Kyushu University, 3-1-1 Maidashi, Higashiku, Fukuoka 812-8582, Japan*
[3]*Department of Biomedical Engineering, Graduate School of Medicine, Kyushu University, 3-1-1 Maidashi, Higashiku, Fukuoka 812-8582, Japan*

Received 11 March 2002; revised 10 June 2002; accepted 19 June 2002

Abstract: In order to reduce the compliance mismatch between the native artery and the artificial graft, we have developed a coaxial double-tubular compliant graft, using multiply micropored segmented polyurethane (SPU) thin films, which mimics the relationship between the intraluminal pressure and vessel internal diameter (P-D) of the native artery (termed "J" curve). The graft was coaxially assembled by inserting a high-compliance inner tube with a heparin-immobilized photocured gelatin coating layer into a low-compliance outer tube with a photocured hydrophilic polymer coating layer. Twenty-eight coaxial double-tubular compliant grafts were implanted into the canine common carotid arteries in an end-to-end fashion for up to 12 months. The overall patency rate was 86% (24/28), and neither rupture nor aneurysmal formation was observed. A neoarterial wall was formed via transanastomotic and transmural tissue ingrowth, resulting in neoarterial tissue formation on the luminal surface and into the intertubular space of the double-tubular graft, accompanied by mainly myofibroblasts and inflammatory cells in the early stage and endothelialization and collagen-rich extracellular matrices in the late stage of implantation. Surrounding-tissue adhesion with the outer tube was prevented by the hydrophilic polymer coating. Although the J curve of the implanted prototype model was preserved 1 month after implantation, the impaired J curves were observed because of tissue ingrowth and tissue adhesion between the outer surface of the inner tube and the surrounding tissues 3 and 6 months after implantation. At 12 months after implantation, however, the implanted coaxial double-tubular graft exhibited high compliance due to biodegradation of the SPU films. © 2003 Wiley Periodicals, Inc. J Biomed Mater Res 65A: 170–181, 2003

Key words: coaxial double-tubular graft; compliance matching; segmented polyurethane; healing process; biodegradation

INTRODUCTION

Arterial tissues including aorta to arteriole are continuously exposed to a dynamic mechanical force such as perpendicular stress, circumferential stress, and shear stress, which are repeatedly driven by cardiac pulsatile output, and these arteries contribute to efficient forward blood flow to peripheral tissues with minimal energy loss because of their unique biomechanical properties[1,2]: large inflation in the low-pressure regions, gradually reduced inflation in the physiological pressure regions, and little inflation in the high-pressure regions, termed the "J" curve.

On the other hand, artificial grafts such as expanded polytetrafluoroethylene (ePTFE; Gore-tex) and polyester-based (Dacron) grafts, which have been widely used clinically for bypass grafting or the replacement of occluded or aneurysmal arterial tissues, are so stiff that the fabricated tubes show little inflation over full-pressure regions. The patency rate after the implantation of a small-diameter artificial graft has been much lower than that of a medium- to large-diameter artificial graft because of an early stage thrombosis and a

Correspondence to: T. Matsuda; e-mail: matsuda@med.kyushu-u.ac.jp
Contract grant sponsor: Promotion Fundamental Studies in Health Science of the Organization for Pharmaceutical Safety and Research (OPSR); contract grant number: 97-15.
Contract grant sponsor: in part by a Grant-in-Aid for Scientific Research from the Ministry of Education, Culture, Sports, Science, and Technology of Japan; contract grant number: A2-12358017 and B2-12470277.

late stage neointimal hyperplasia.[3–6] Among the many factors determining the patency of the small-diameter artificial grafts, the compliance mismatch between the native artery and the artificial grafts has been discussed as a major detrimental factor of graft failure.[1,5,7–10] Thrombus formation and neointimal hyperplasia on the surface of the small-diameter artificial graft become more critical factors for graft failure than those of the medium- to large-diameter artificial graft, because the effective flow area of the small-diameter artificial graft must be much smaller when the same amount of thrombus or neointimal hyperplasia is generated. In addition, the difference in mechanical properties between a native artery and an artificial graft induces hemodynamical flow disturbance and stress concentration near the anastomoses, causing further thrombus formation and neointimal hyperplasia.[1,5,7–10] Therefore, the small-diameter artificial graft essentially requires compliance matching with the native arteries as much as possible.

We reported new design concept based on biomechanical design criteria and fabricated a prototype small-diameter graft of a unique structure[11]: a coaxial double-tubular compliant graft biomimicking the J curve of canine common carotid arteries using micropored segmented polyurethane (SPU) films. SPU has long been used as a material for the artificial heart (e.g., diaphragms or valves), because of proven physical characteristics such as highly flexible elastomer and excellent durability against cyclic stretching. The coaxial double-tubular compliant graft was assembled by inserting the high-compliance inner tube into the low-compliance outer tube (Fig. 1). Upon increasing the intraluminal hydrodynamic pressure, the inner tube inflates markedly in the low-pressure regions (Fig. 1, phase A to B), and after the inner tube comes in contact with the outer tube (Fig. 1, phase B), both tubes inflate together gradually in the high-pressure regions (Fig. 1, phase C). This mechanical property mimicks the J curve of the native artery. The wall thickness, diameter and pore density (relative area of micropores), which are the principal parameters determining the pressure-dependent diameter change, were adjusted to meet the design criteria of the graft (target vessel was canine carotid arteries: inner diameter, 4.0 mm; averaged from eight arteries) and were 50 μm, 4.5 mm, and 35.1% for the inner tube, and 100 μm, 5.5 mm, and 15.0% for the outer tube, respectively (Fig. 2). This fabricated coaxial double-tubular graft exhibited the J curve mimicking that of target canine carotid arteries. The transition point was set within the physiological pressure range (100 mmHg).

In this article, the surface processing aiming at reduced thrombus formation on the luminal surface of the inner tube in the early stage of implantation and prevention of tissue-mediated adhesion between the inner and outer tubes and between the outer tube and the surrounding tissues, was conduced by photochemical grafting. Upon implantation into canine carotid arteries, morphogenesis and compliance changes were investigated. The perspective of the coaxial double-tubular graft and the shortcomings of the current technology were discussed.

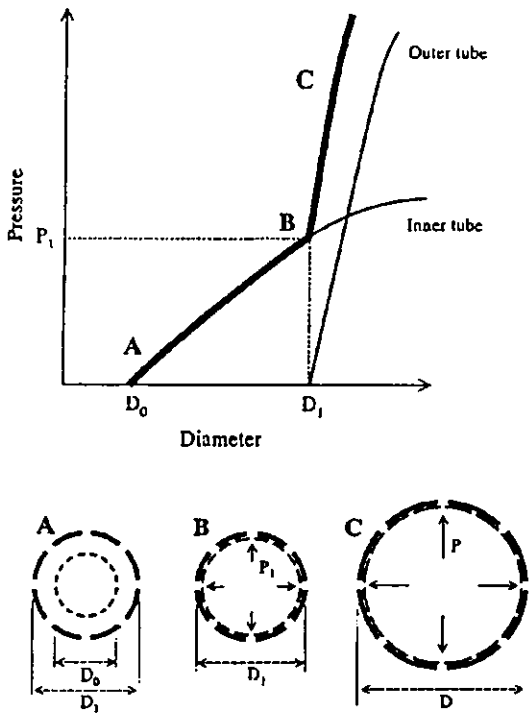

Figure 1. Design concept of the coaxial double-tubular compliant graft. Top: the conceptual pressure-diameter relationship of the coaxial double-tubular graft. Bottom: the short-axis views of the coaxial double-tubular graft, depending on the intraluminal pressure. Phase A: at zero pressure; phase B: at P_1 (contact phase); phase C: at given P (high-pressure regions). The inner tube inflates rapidly in the low-pressure regions (phase A to B). After the inner tube comes in contact with the outer tube (phase B), both tubes inflate together gradually (phase C).

MATERIALS AND METHODS

Fabrication of coaxial double-tubular compliant graft

The design criteria and the detailed fabrication procedures of the coaxial double-tubular compliant graft were reported previously.[11] Briefly, our graft was assembled by inserting a high-compliance inner tube into a low-compliance outer tube. The materials used were multiply micropored segmented polyurethane thin films (Cardiomat 610, Zeon Kasei Co., Ltd., Tokyo, Japan). It is claimed by the manufacture that Cardiomat 610, a segmented poly(urethane-ether) was prepared from poly(teramethylene glycol), 1,4-diphenyl methane diisocyanate and 1,4-butanediol

	Diameter	Pore Density	Wall Thickness
Inner tube	4.5 mm	35.1%	50 μm
Outer tube	5.5 mm	15.0%	100 μm

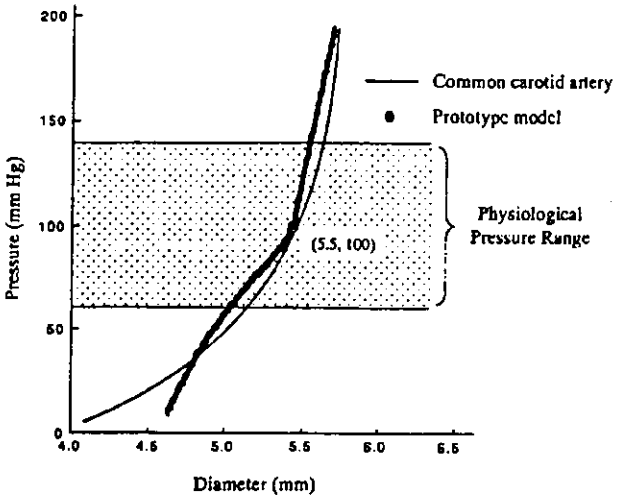

Figure 2. Design criteria and pressure-diameter relationship of the prototype model of the coaxial double-tubular graft. The pressure-diameter relationships of the prototype model matched well with that of the common carotid artery in the intermediate and higher pressure regions, and the transition point was set within the physiological pressure range.

(chain extender). The material descriptions including dimensions are listed in Figure 2 and shown in Figure 3.

A surface coating was applied to the graft using a photografting technique previously developed by us. The outer and inner surfaces of the inner tube were coated with a mixed aqueous solution of 2 wt % photoreactive gelatin [benzophenone-derivatized gelatin: number of benzophenone groups is 29.9 per gelatin molecule (molecular weight: 9.5×10^4)] and 1 wt % heparin (Wako Pure Chemicals Inc., Osaka, Japan) and subsequently photocured by ultraviolet (UV) light irradiation from a mercury arc lamp (H-400P, Toshiba, Tokyo, Japan; $\lambda > 270$ nm; intensity, 0.14 mW/cm^2).[12–15] The outer and inner surfaces of the outer tube were coated with 1% aqueous solution of a photoreactive hydrophilic polymer, poly(*N,N*-dimethylacrylamide-*co*-m-azidostyrene) (azidostyrene content: 10 mol %; molecular weight: 2.0×10^4) and subsequently photocured by UV light irradiation.[16]

Animal models

Twenty-eight coaxial double-tubular compliant grafts were bilaterally implanted into the common carotid arteries of 14 adult mongrel dogs (average weight, 28.5 ± 2.2 kg; range, 25–35 kg, Table I). All animals received care according to the "Principles of Laboratory Animal Care" (formulated by the National Society for Medical Research) and the "Guide for the Care and Use of Laboratory Animals" (NIH publication no. 86-23, revised 1985).

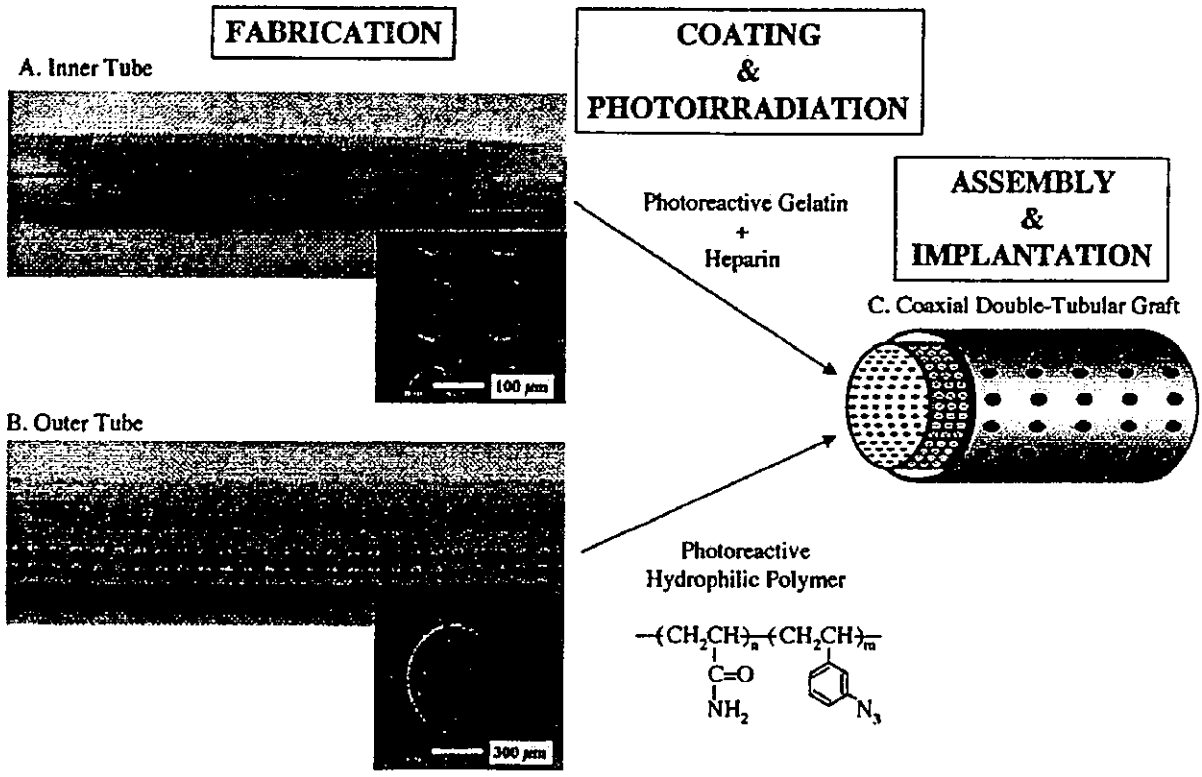

Figure 3. Fabrication process of the coaxial double-tubular graft. The inner and outer tubes were fabricated and coated separately, and the coaxial double-tubular graft was assembled by inserting the inner tube into the outer tube.

TABLE I
Patency as a Function of Implantation Period

Implantation Period (month)	Body Weight (kg)	No. of Patent Grafts/ No. of Implanted Grafts
1	28.5 ± 1.0	7/8 (88%)
3	29.7 ± 3.5	6/6 (100%)
6	28.0 ± 1.7	5/6 (83%)
12	28.0 ± 2.7	6/8 (75%)
Average	28.5 ± 2.2	24/28 (86%)

Graft implantation

General anesthesia was induced by injection of intramuscular ketamine (Ketaral 50, Sankyo Co., Ltd., Tokyo, Japan; 15 mg/kg) and intravenous pentobarbital (Nembutal, Dainippon Pharmaceutical Co., Ltd., Osaka, Japan; 10 mg/kg) and maintained by intermittent injection of pentobarbital. Bilateral para-tracheal incisions were made along the trachea, and both common carotid arteries were dissected, which yielded a segment approximately 10 cm in length. After intravenous injection of heparin (Novo Heparin, Novo Nordisk Pharmaceuticals, Copenhagen, Denmark; 100 U/kg), the arteries were crossclamped 20 mm away from the anastomoses, and a segment 30 mm long was resected. The coaxial double-tubular graft was interposed by means of end-to-end anastomosis (Fig. 4). The anastomoses of the inner tube were constructed with 12 interrupted 7-0 polypropylene sutures (Nespilene, Azwell Co., Ltd., Osaka, Japan) on each side, and the outer tube that was placed outside of the inner tube over the anastomosis was roughly fixed to the adventitia of the adjacent native artery. Neither antiplatelet nor anticoagulant agents were administered except for the intraoperative heparin injection.

Histological examination

All grafts were fixed *in situ* with 20% formaldehyde and 4% glutaraldehyde except for the grafts subjected to measurement of the compliance (P-D relationship), which were fixed after the measurement. Specimens for light microscopic examination were stained with hematoxylin-eosin, Masson's trichrome, and Elastica van Gieson to observe the time-dependent changes of neoarterial structure and wall thickness of the grafts after implantation. For immunohistochemical staining, the antibodies against the smooth muscle α-actin (1A4, DAKO Corp., Glostrup, Denmark) and the von Willebrand factor (A082, DAKO Corp.) were used to identify the smooth muscle cells (SMCs) and the endothelial cells (ECs), respectively. Specimens for scanning electron microscopic observation were postfixed with 1% osmium tetroxide, dehydrated in graded series of ethanol, critical point dried, and sputter-coated with osmium to identify the endothelial ingrowth of the luminal surface of the grafts. The surfaces of the SPU materials of the retrieved outer tubes were also observed using a scanning electron microscope (SEM: JSM-6301F, JEOL, Tokyo, Japan).

Measurements of P-D relationship and compliance

The P-D relationships of the retrieved grafts with adjacent arteries at 1, 3, 6, and 12 months after implantation were measured using a digital X-ray imaging system and a pressure transducer as previously reported.[17] Briefly, one end of a vessel segment was cannulated to a fixed stainless steel connector for pressure loading and the other to a sliding connector, and the vessel was restored to *in situ* length in a bath filled with Krebs-Ringer solution held at 37°C. The vessel was gradually inflated with a pressurized contrast medium (Iomeron 350, Eisai Co., Ltd., Tokyo, Japan) using a syringe pump, recording the intraluminal pressures from 0 to ~200 mmHg. An X-ray digital fluoro-imaging system (series 9600, OEC Medical Systems Inc., Salt Lake City, UT) was used for obtaining the intraluminal radiographs of the vessel, and real-time digital images were recorded on a digital videocassette tape. The P-D relationships at the middle portion of the grafts were measured using an NIH Image software (Version 1.59, public domain software). The details of the procedure were described in our previous article.[17]

Compliance changes were evaluated with the stiffness parameter (β value) determined from the following equation[18,19]:

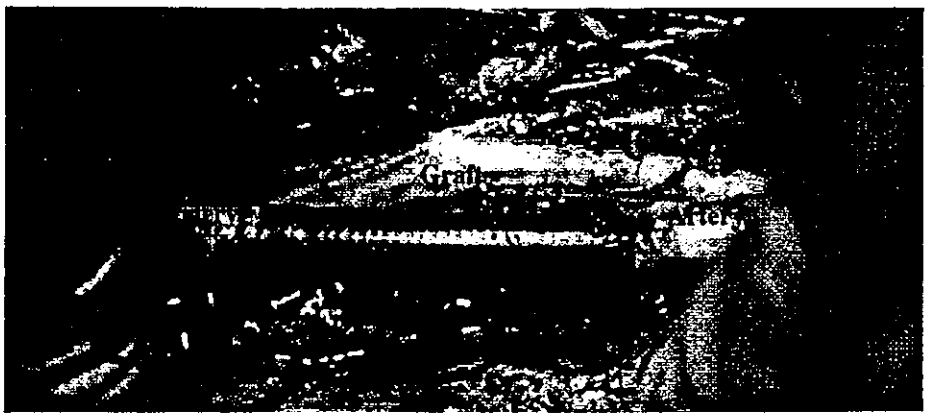

Figure 4. Operative findings of the coaxial double-tubular grafts. The grafts were implanted into the canine common carotid arteries in an end-to-end fashion.

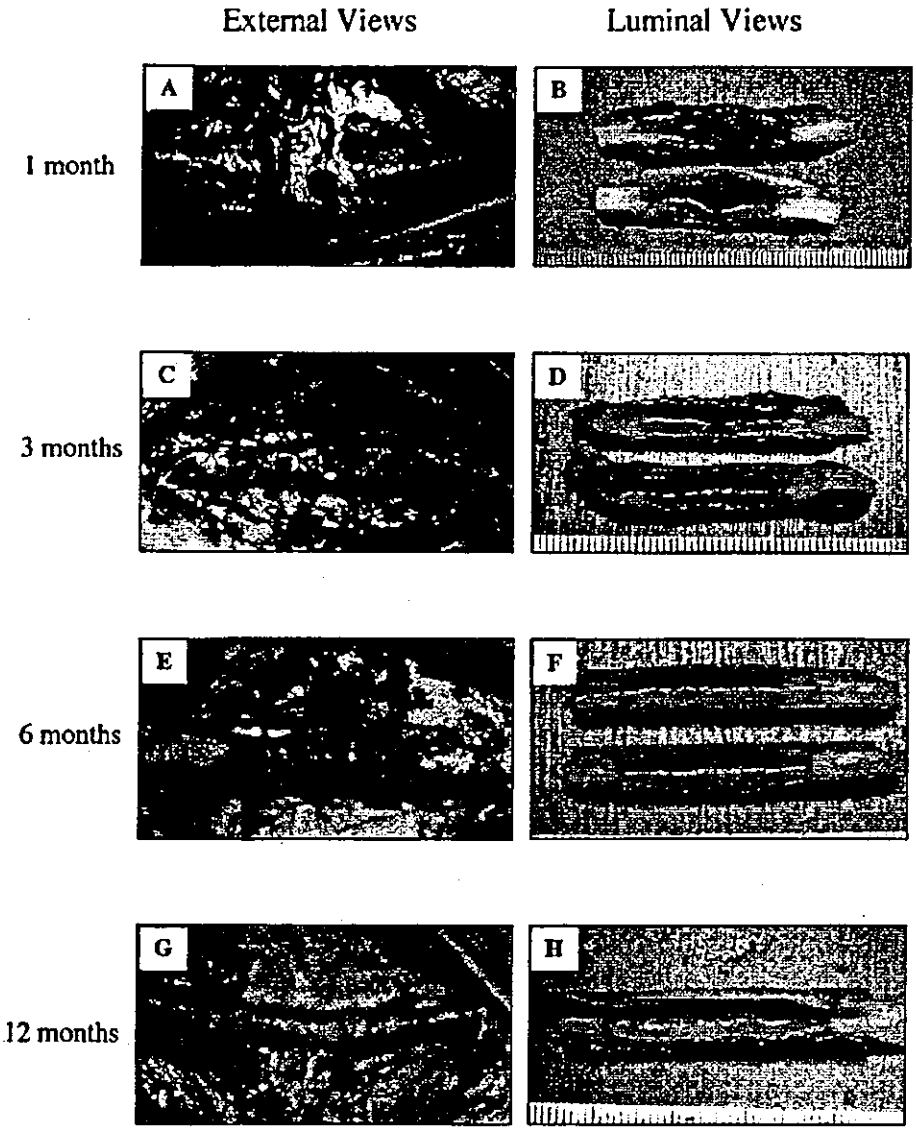

Figure 5. The external and luminal views of the grafts after implantation.

$$\ln (P/Ps) = \beta(D/Ds - 1) \quad (1)$$

where Ps and Ds are the standard intraluminal pressure (100 mmHg in this study) and the external diameter at Ps, respectively. P is the intraluminal pressure and D is the external diameter at P.

RESULTS

The fabrication procedure of double-tubular graft is schematically shown in Figure 3. The diameters of inner and outer tubes were 4.5 and 5.5 mm, respectively. For both tubes, the inner and outer surfaces were photografted with a respective photoreactive substance. The inner tube was coated with a photocured heparin-immobilized gelatin layer, and the outer tube was photografted with a hydrophic polymer, poly(*N,N*-dimethylacrylamide) partially derivatized with a photoreactive group (phenylazide). Both surface processing technologies and materials were described in our previous articles.[12–16] These grafts were bilaterally implanted into canine common carotid arteries up to 12 months. Figure 4 shows a photograph of the surgical operation. When anastomosed and blood-circulated, the periodic cycles of inflation and deflation of the graft were noted, indicating that pulsatile blood flow was taking place in the implanted graft.

Patency and macroscopic appearance

Twenty-four of the 28 grafts were patent at the moment of explantation (overall patency rate: 86%;

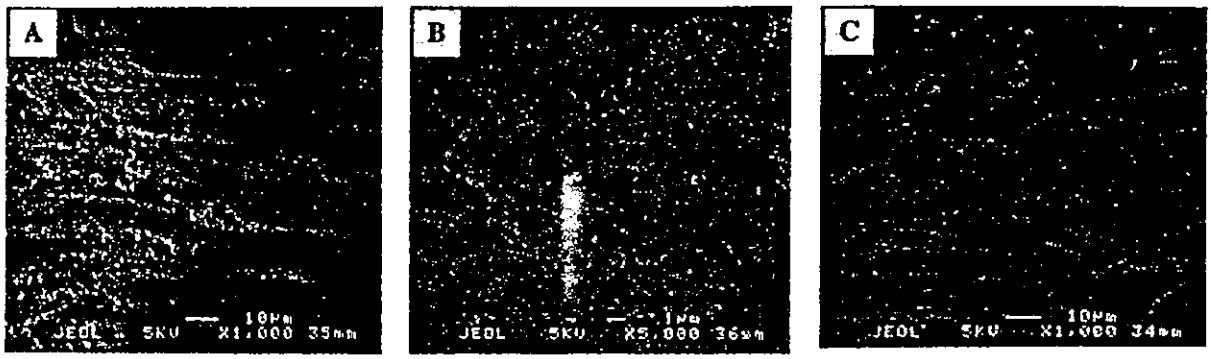

Figure 6. Scanning electron microscopic findings of the luminal surface of the implanted graft. (A) Anastomosis portion at 1 month after implantation (original magnification, ×1000). (B) Middle portion at 3 months after implantation (original magnification, ×5000). (C) Middle portion at 6 months after implantation (original magnification, ×1000).

Table I). Figure 5 shows the external and luminal views of the implanted graft at various times. Neither rupture nor aneurysmal formation was observed even at 12 months after implantation. Tissue adhesion around the graft was most massive at 1 month after implantation [Fig. 5(A)], but the degree of adhesion reduced gradually with the implantation period [Fig. 5(C,E,G)]. The outer tube photografted with a hydrophilic polymer could be retrieved easily without adhesion between the inner and outer tubes in all observation periods. The intertubular space between the inner and outer tubes was filled with ingrowth tissues that migrated from the tissues surrounding the graft or from the host arteries.

In the luminal views, thrombus formation was observed at 1 and 3 months after implantation [Fig. 5(B,D)]. At 6 and 12 months after implantation, the luminal surface was almost covered with glistening and milky-white neointima with little thrombus and neointimal hyperplasia [Fig. 5(F,H)].

Implantation-period-dependent morphogenesis

SEM observation shows that the ECs infiltrated sequentially from both proximal and distal stumps of the host artery into the graft surface beyond the anastomoses [Fig. 6(A)]. The endothelializing front was positioned at ~3 mm from the anastomoses at 1 month after implantation, and at ~7 mm at 3 months after implantation. At 1 and 3 months after implantation, the luminal surface of the graft where ECs were not found was covered with the thrombus or fibrin [Fig. 6(B)]. At 6 months after implantation, however, the luminal surface was completely covered with ECs [Fig. 6(C)].

The neoarterial wall was reconstructed by tissue ingrowth from the arterial stumps and from the surrounding tissues through the micropores of the grafts. The tissue ingrowth inside the inner tube and the tissue ingrowth into the intertubular space between the inner and outer tubes were defined here as the neointima and the neomedia, respectively. At 1 month after implantation, the neointima and the neomedia near the anastomosis were filled with myofibroblast-rich cells and inflammatory cells [Fig. 7(A), 8, and 9(A)], and fresh thrombus was attached to the luminal surface of the middle portion of the graft [Figs. 7(E) and 9(E)]. At 3 months after implantation, the neointima and the neomedia near the anastomosis began to be replaced with collagen-rich extracellular matrices [Figs. 7(B) and 9(B)], although fibrin was attached to the luminal surface of the middle portion of the graft [Figs. 7(F) and 9(F)]. At 6 months after implantation, the neointima and the neomedia were almost replaced with extracellular matrices, and the cellular components were localized at the luminal side of the neointima [Figs. 7(C,G) and 9(C,G)]. At 12 months after implantation, well-aligned smooth muscle cell layers, the thickness of which were approximately 50 to 80 μm, were observed beneath the intima [Figs. 7(D,H), 9(D,H), and 10(A,B)], although elastic fibers were not observed among those layers [Fig. 10(C)]. Also, the luminal surface of the neointima was fully covered with ECs [Fig. 10(D)].

Figure 11 shows the time-dependent change of wall thickness. The neointimal wall thickness at para-anastomosis of the grafts at 3 months after implantation was the largest (512 ± 41 μm) and decreased at 6 and 12 months after implantation (414 ± 54 μm at 6 months, and 313 ± 48 μm at 12 months). The neointimal wall thickness in the middle portion of the grafts became larger with time, reaching approximately 315 ± 30 μm at 12 months after implantation [Fig. 11(A)]. On the other hand, the neomedial wall thicknesses at para-anastomosis of the grafts were significantly larger than those in the middle portion in all observation periods except that at 3 months [Fig. 11(B)].

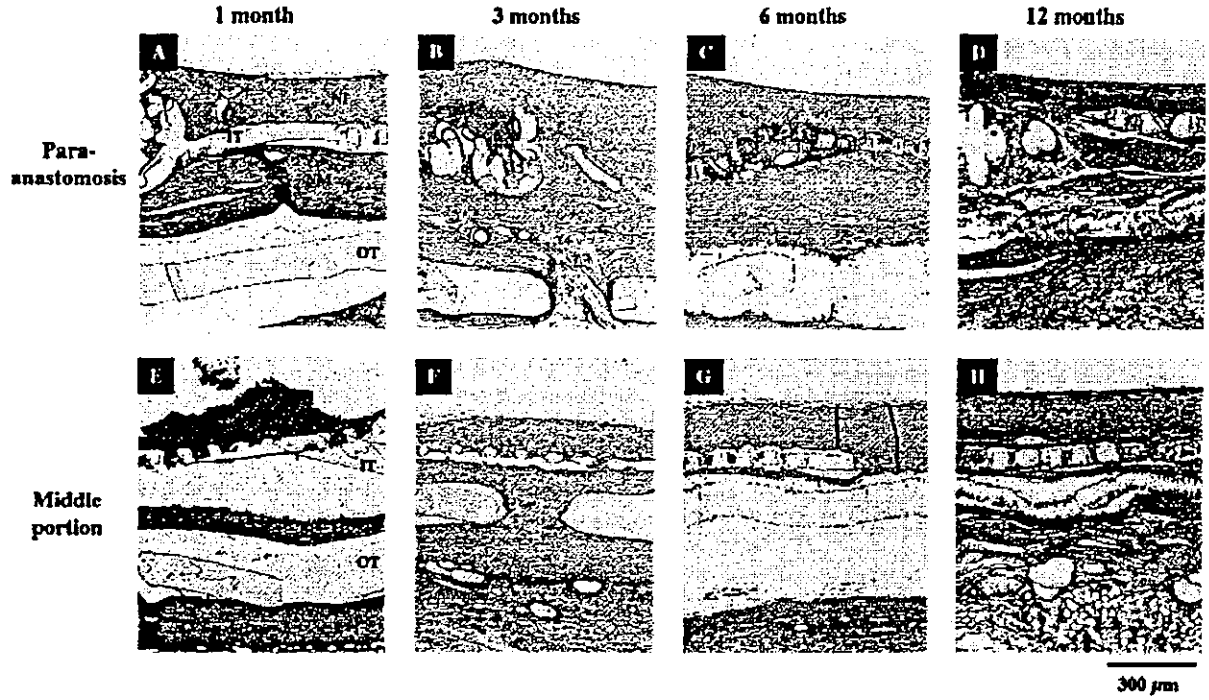

Figure 7. Longitudinal sections at the para-anastomosis and the middle portion of the grafts after implantation. The sections were stained with hematoxylin-eosin. IT, inner tube; OT, outer tube; NI, neointima; NM, neomedia. Original magnification, ×40.

Compliance changes and material deterioration

The P-D relationships after implantation are shown in Figure 12. The P-D relationship at 1 month after implantation exhibited the J curve but became steeper at 3 and 6 months after implantation. The J curve was restored only within the low-pressure regions. However, the J curve was observed again at 12 months after implantation. This curve closely resembled that of the native arteries: large inflation in the low-pressure regions and gradual inflation in the high-pressure regions. The stiffness parameter (β value), calculated from Equation (1), is also shown in Figure 12: the β value of the preimplanted graft was 9.2, which was

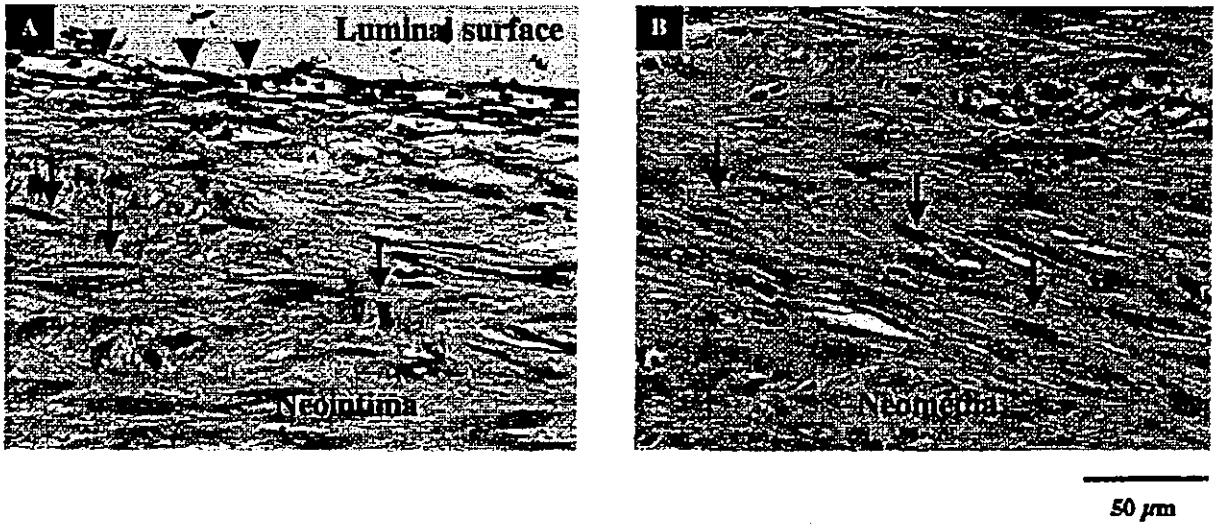

Figure 8. Microscopic findings at the para-anastomosis of the graft at 1 month after implantation (hematoxylin-eosin staining). Arrows and arrowheads indicate myofibroblasts and inflammatory cells, respectively. Original magnification, ×400.

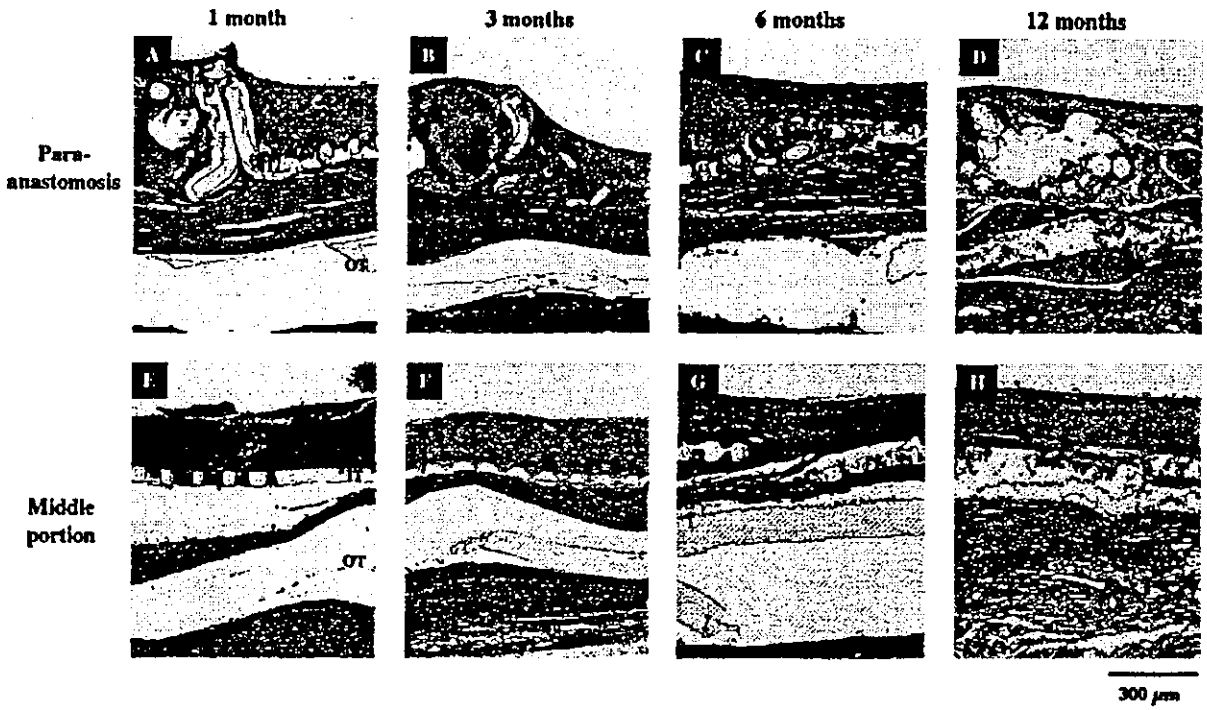

Figure 9. Longitudinal sections at the para-anastomosis and the middle portion of the grafts after implantation. The sections were stained with Masson's trichrome. IT, inner tube; OT, outer tube; NI, neointima; NM, neomedia. Original magnification, ×40.

comparable to that of the native artery but with longer implantation periods; the β value increased to 51.4 at 6 months after implantation but decreased to 19.6 at 12 months after implantation.

SEM observations of the surfaces of the material (SPU) are shown in Figure 13. The surface and edge of the fabricated micropores before implantation were fairly smooth [Fig. 13(A)]. However, the surface gradually became rougher with time [Figs. 13(B–D)], and many deep cracks were observed around the fabricated micropores at 12 months after implantation [Fig. 13(D)], strongly indicating that the SPU film degraded with time, resulting in the loss of integrity leading to the decrease of mechanical strength of the SPU film of the tube.

DISCUSSION

Despite much effort and various approaches as well as numerical attempts to develop vitally functioning small-diameter artificial grafts for many years, a majority of the research works have shown only the partial improvements including surface-biocompatible modification or the quality of the graft material, and only a few research groups have continued to develop novel small-diameter artificial grafts in terms of material, surface, and structural designs.[20–22]

The structural components of native arteries are mainly cellular elements (SMCs and ECs) and connective tissue elements (elastic and collagenous fibers). Among these components, the latter elements contribute to the mechanical strength of the native artery and the unique mechanical property of the native artery (termed J curve): an artery easily inflates in the low-pressure regions (0 to ~60 mmHg), moderately inflates in the physiological pressure regions (~60–140 mmHg), and hardly inflates in the high-pressure regions (approximately >140 mmHg). The single synthetic elastomeric tube made of SPU generally exhibits an "inverse J" curve in the P-D relationship due to creep characteristics of the elastomeric film, which occur under high stretching conditions. To overcome this problem, our conceptual design and fabrication technology are based on the coaxial double-tubular graft, that was assembled by two different types of elastomeric tubes: the inner tube has high-compliance and the outer tube has low-compliance, and theoretically and experimentally this type of graft mimicked the J curve, as shown in Figure 2.

Although the J curve in the P-D relationship was realized by the optimal selections of material, structural, and fabrication parameters as described in our previous article, one potential problem that remains to be solved is the tissue adhesion between the inner and outer tubes upon tissue ingrowth and that be-

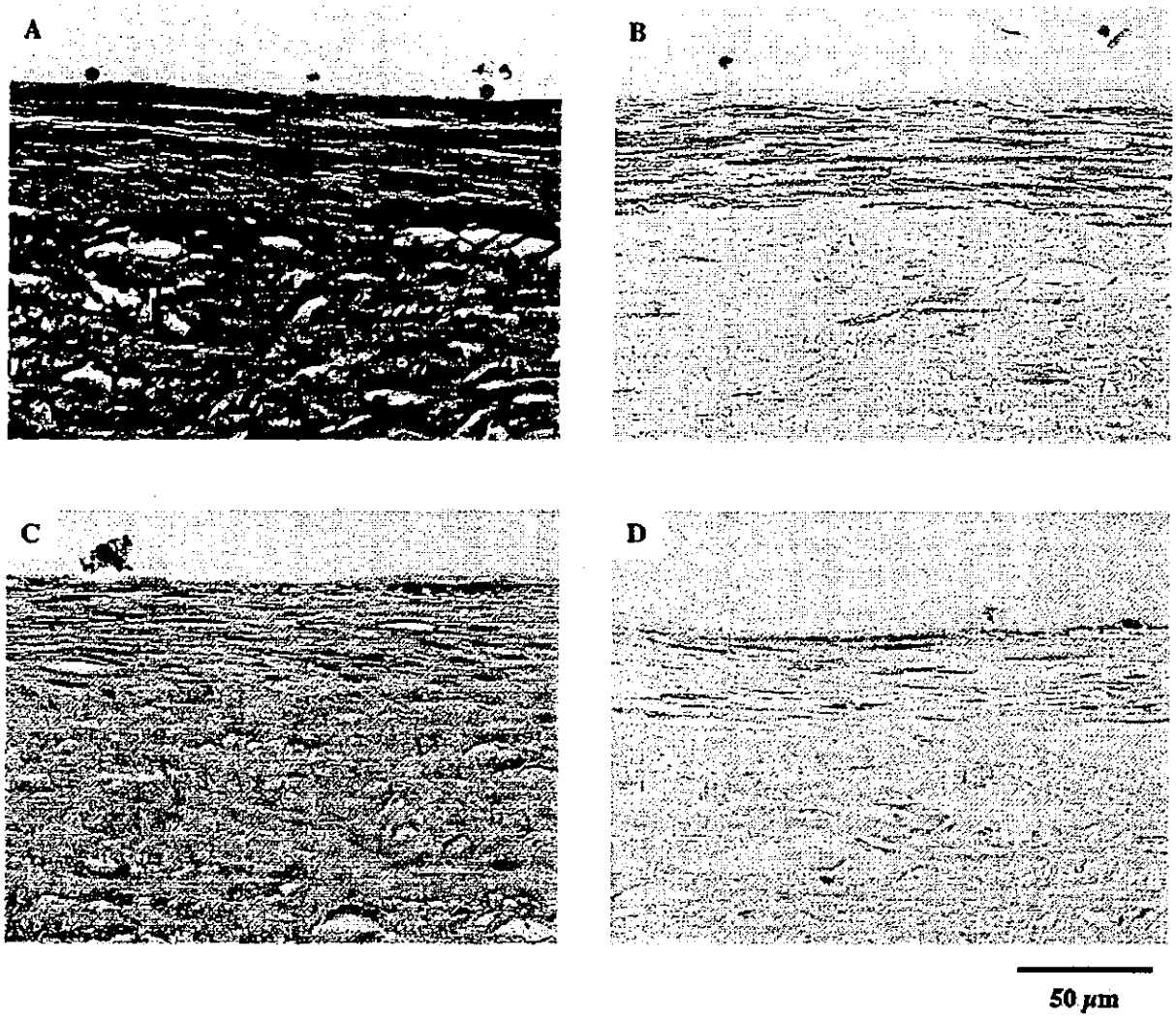

Figure 10. Longitudinal sections at the middle portion or the graft at 12 months after implantation. (A) Masson's trichrome staining. (B) Staining for smooth muscle α-actin. (C) Elastica van Gieson's staining. (D) Staining for von Willebrand factor.

tween the outer tube and the surrounding tissue. If these occur during the implantation period, the two tubes would unify to behave as a single tube for the former case or show considerably reduced compliance for the latter case. To circumvent or solve these problems, we performed surface photoprocessing of these tubes, and this led to long-term patency and restoration of compliance. The coating material was

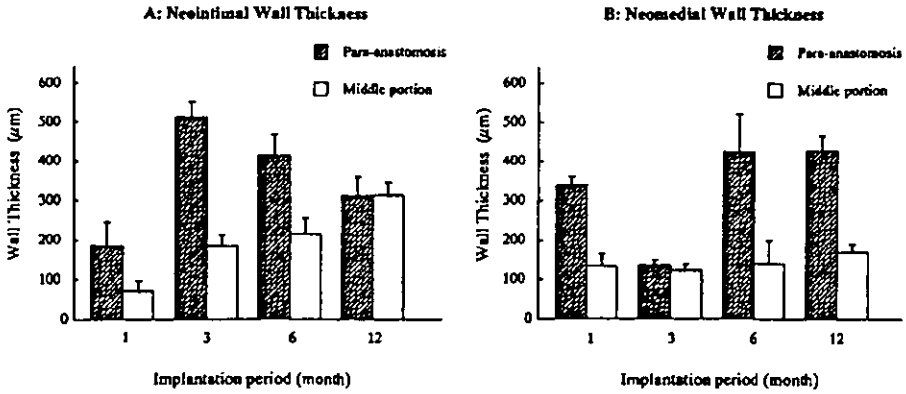

Figure 11. Time-dependent changes of neointima (A) and neomedia (B) at the para-anastomosis and the middle portion of the grafts after implantation.

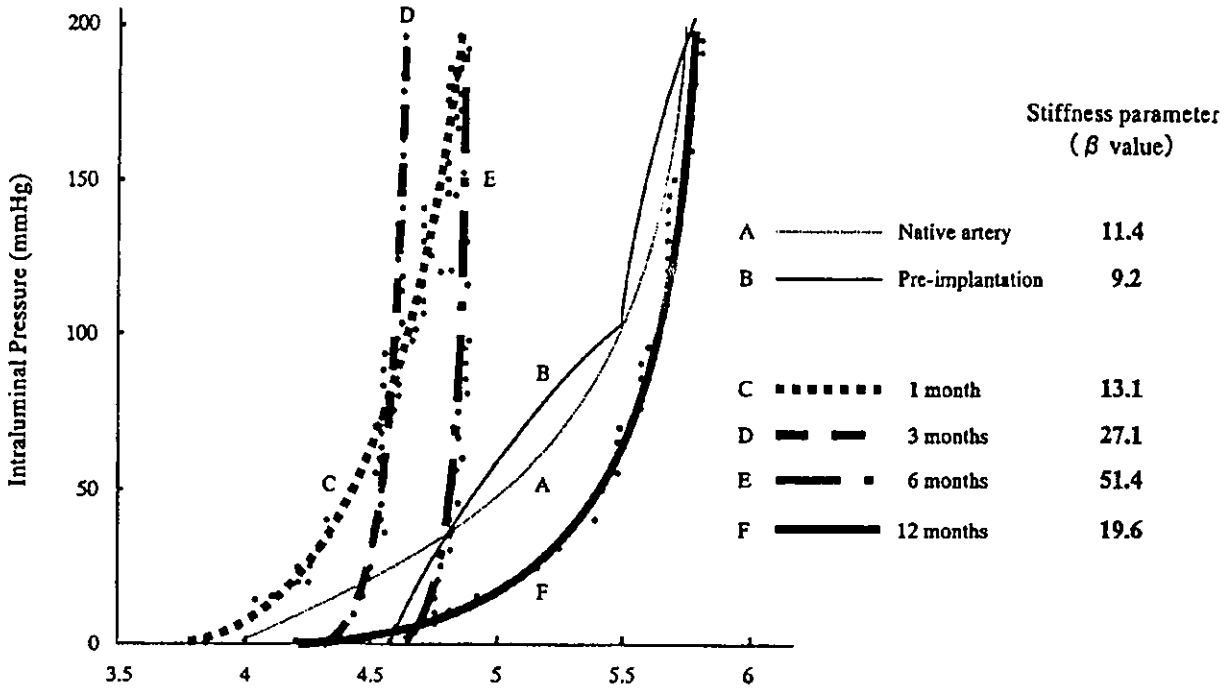

Figure 12. Time-dependent changes of the pressure-diameter relationship of the grafts and the stiffness parameters (β values) after implantation.

photoreactive gelatin mixed with heparin for the inner tube and photoreactive hydrophilic polymer for the outer tube. The photografting of these substances on respective tubes by UV light irradiation resulted in the formation of covalently bonded graft layers.

Although the patency rate was comparably high (~86%), thrombus formation was partially observed on the luminal surface of the graft at 1 and 3 months after implantation. This result indicated that although the heparin immobilized in and released from the photoreactive gelatin layer appears to help suppress thrombus formation, its loading amount appears to be insufficient for preventing thrombus formation. The luminal surface was completely endothelialized at 6 months after implantation. On the other hand, the outer tube photografted with the nonionically hydrophilic polymer eventually prevented the adhesion between the surface and the ingrown tissues. However, the neoarterial tissue, which regenerated in the interspace between the outer and inner tubes through the micropores of the outer tube, adhered to the outer surface of the inner tube. In addition, foreign body reactions such as encapsulation or fibrosis occurred at the outer surface of the outer tube. These combined effects appear to be responsible for the stiffening of the implanted graft with increasing implantation period (Fig. 12). The major components of the neoarterial tissue were myofibroblasts and inflammatory cells in the early phase, and collagen-rich extracellular matrices were produced with time. This appears to be the normal wound healing process. However, although well-aligned SMC layers beneath the intima were observed, the elastic fibers were not produced even at 12 months after implantation.

Increased stiffening of the implanted grafts and impaired J curve were noted with time, probably because of the regenerated neoarterial wall and tissue adhesion to the inner tube, as described above. On the other hand, the revert-back J curve observed at 12 months after implantation was closely associated with the deterioration of SPU, which was evidenced by crack development at laser-ablated micropores and its radial propagation, resulting in the deterioration of mechanical properties. In fact, the mechanical strength of the micropored SPU films retrieved at 12 months after implantation decreased approximately to one-tenth of that of the preimplanted SPU films (data not shown). This may be due to stress concentration at the edge of micropores caused by continuously loaded pulsatile stress as well as material deterioration derived from high-energy pulsed laser ablation at the edge. This material deterioration was not expected because segmented polyurethane, Cardiomat 610, has a well-proven decrability when it has been used for fabrication of commercial blood pumps such as intra-aortic blood pump and left ventricular device. However, the structural and concomitant mechanical deterioration observed in this study may imply that biodegradation rate is much faster in tissues than in circulating blood and that stress-concentration generated during fabrication enhances biodegradation.

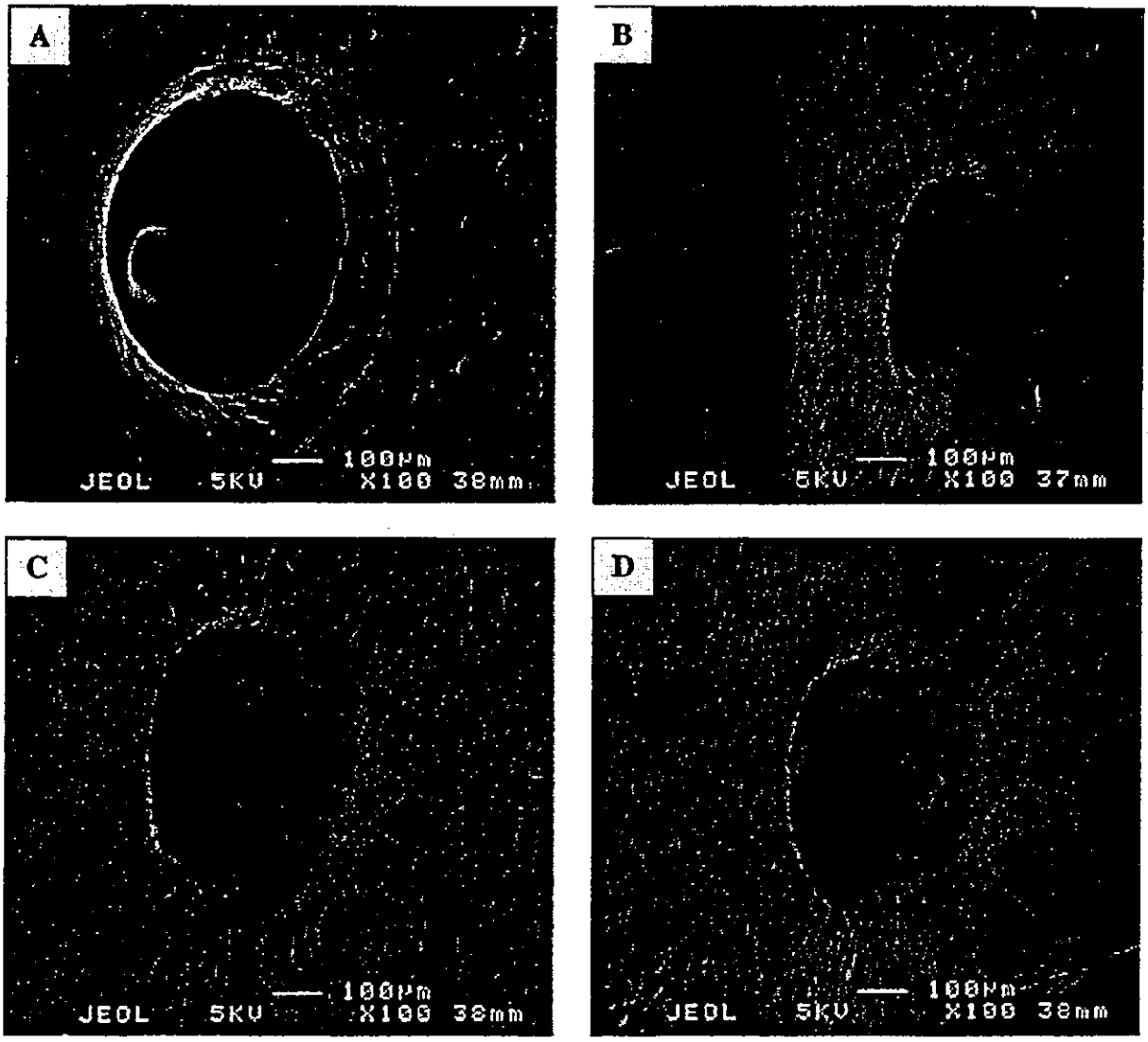

Figure 13. Scanning electron microscopic findings of the surface of the segmented polyurethane films before and after implantation. (A) At preimplantation. (B) At 3 months after implantation. (C) At 6 months after implantation. (D) At 12 months after implantation. Original magnification, ×100.

These two effects appear to synergistically operate in this particular application. Therefore, a more durable segmented polyurethane using polycarbonate as a soft segment must be used for fabrication of coaxial double-tubular artificial grafts.

The concept and fabrication of coaxial double-tubular compliant grafts composed of very thin multiply micropored SPU films are quite unique; these were designed and constructed from biomechanical and biomaterial viewpoints. The J curve in the P-D relationship was realized in the early stage of implantation. However, the occurrence of an impaired P-D relationship with increasing implantation period indicates that manipulation of tissue ingrowth and strict prevention of tissue adhesion are essential for this system. The key issues to be resolved in future study are surface processing technology leading to more precise control of tissue ingrowth including encapsulation and tissue adhesion prevention, and material design for producing highly durable SPU. Once these are materialized, this uniquely structured artificial graft will function well to exhibit biomechanically functional adaptation and controlled tissue architecture.

References

1. Kinley CE, Marble AE. Compliance: a continuing problem with vascular grafts. J Cardiovasc Surg 1980;21:163–170.
2. Burton AC. Relation of structure to function of the tissues of the wall of blood vessels. Physiol Rev 1954;34:619–642.

3. Friedman SG, Lazzaro RS, Spier LN, Moccio C, Tortolani AJ. A prospective randomized comparison of Dacron and polytetrafluoroethylene aortic bifurcation grafts. Surgery 1995;117:7–10.
4. Prager M, Polterauer P, Bohmig HJ, Wagner O, Fugl A, Kretschmer G, Plohner M, Nanobashvili J, Huk I. Collagen versus gelatin-coated Dacron versus stretch polytetrafluoroethylene in abdominal aortic bifurcation graft surgery: results of a seven-year prospective, randomized multicenter trial. Surgery 2001;130:408–414.
5. Pevec WC, Darling RC, L'Italien GJ, Abbott WM. Femoropopliteal reconstruction with knitted, nonvelour Dacron versus expanded polytetrafluoroethylene. J Vasc Surg 1992;16:60–65.
6. Devine C, Hons B, McCollum C. Heparin-bonded Dacron or polytetrafluoroethylene for femoropopliteal bypass grafting: a multicenter trial. J Vasc Surg 2001;33:533–539.
7. Abbott WM, Megerman J, Hasson JE, L'Italien G, Warnock DF. Effect of compliance mismatch on vascular graft patency. J Vasc Surg 1987;5:376–382.
8. Kidson IG, Abbott WM. Low compliance and arterial graft occlusion. Circulation 1978;58(Suppl):I1–I4.
9. Qiu Y, Tarbell JM. Computational simulation of flow in the end-to-end anastomosis of a rigid graft and a compliant artery. ASAIO J 1996;42:M702–M709.
10. Stewart SF, Lyman DJ. Effects of a vascular graft/natural artery compliance mismatch on pulsatile flow. J Biomech 1992; 25:297–310.
11. Sonoda H, Takamizawa K, Nakayama Y, Yasui H, Matsuda T. Small-diameter compliant arterial graft prosthesis: Design concept of coaxial double tubular graft and its fabrication. J Biomed Mater Res 2001;55:266–276.
12. Nakayama Y, Ishibashi K, Matsuda T. Benzophenone-derivatized gelatin as photocurable hemostatic glue: Gelation characteristics by an excimer laser irradiation and its in vivo performance. Jpn J Artif Organs 1995;24:102–105.
13. Doi K, Nakayama Y, Matsuda T. Novel compliant and tissue-permeable microporous polyurethane vascular prosthesis fabricated using an excimer laser ablation technique. J Biomed Mater Res 1996;31:27–33.
14. Doi K, Matsuda T. Enhanced vascularization in a microporous polyurethane graft impregnated with basic fibroblast growth factor and heparin. J Biomed Mater Res 1997;34:361–370.
15. Doi K, Matsuda T. Significance of porosity and compliance of microporous, polyurethane-based microarterial vessel on neoarterial wall regeneration. J Biomed Mater Res 1997;37:573–584.
16. Matsuda T, Inoue K, Sugawara T. Development of micropatterning technology for cultured cells. ASAIO Trans 1990;36: M559–62.
17. Sonoda H, Urayama S, Takamizawa K, Nakayama Y, Uyama C, Yasui H, Matsuda T. Compliant design of artificial graft: compliance determination by new digital X-ray imaging system-based method. J Biomed Mater Res 2002;60:191–195.
18. Hayashi K, Nakamura T. Material test system for the evaluation of mechanical properties of biomaterials. J Biomed Mater Res 1985;19:133–144.
19. Hayashi K, Handa H, Nagasawa S, Okumura A, Moritake K. Stiffness and elastic behavior of human intracranial and extracranial arteries. J Biomech 1980;13:175–184.
20. van der Lei B, Nieuwenhuis P, Molenaar I, Wildevuur CR. Long-term biologic fate of neoarteries regenerated in microporous, compliant, biodegradable, small-caliber vascular grafts in rats. Surgery 1987;101:459–467.
21. Okoshi T, Soldani G, Goddard M, Galletti PM. Penetrating micropores increase patency and achieve extensive endothelialization in small diameter polymer skin coated vascular grafts. ASAIO J 1996;42:M398–401.
22. Hsu S, Kambic H. On matching compliance between canine carotid arteries and polyurethane grafts. Artif Organs 1997;21: 1247–1254.

Available online at www.sciencedirect.com
SCIENCE DIRECT®
Biomaterials 24 (2003) 2295–2302
Biomaterials
www.elsevier.com/locate/biomaterials

Fabrication of endothelial progenitor cell (EPC)-seeded intravascular stent devices and in vitro endothelialization on hybrid vascular tissue

Toshihiko Shirota[a,b], Hisataka Yasui[b], Hiroaki Shimokawa[c], Takehisa Matsuda[a,*]

[a] Department of Biomedical Engineering, Graduate School of Medicine, Kyushu University, 3-1-1 Maidashi, Higashi-ku, Fukuoka 812-8582, Japan
[b] Department of Cardiac Surgery, Graduate School of Medicine, Kyushu University, 3-1-1 Maidashi, Higashi-ku, Fukuoka 812-8582, Japan
[c] Department of Cardiovascular Medicine, Graduate School of Medicine, Kyushu University, 3-1-1 Maidashi, Higashi-ku, Fukuoka 812-8582, Japan

Received 8 November 2002; accepted 18 December 2002

Abstract

Rapid re-endothelialization at an atherosclerotic lesion after balloon inflation or stent deployment may be essential for reducing or preventing local thrombus formation and restenosis. In order to prevent these complications via enhanced rapid re-endothelialization, we fabricated two types of endothelial progenitor cell (EPC)-seeded intravascular stent devices. One was a photocured gelatin-coated metallic stent, and the other was a microporous thin segmented polyurethane (SPU) film-covered stent on which photocured gelatin was coated. Both devices were seeded with ex vivo expanded EPCs obtained from canine peripheral blood. Seeded EPCs formed confluent monolayers onto surfaces of both photocured gelatin-coated stent struts and SPU film, and a majority of cells remained on surfaces of stents after stent expansion. The EPC-seeded stent was expanded in a tubular hybrid vascular medial tissue composed of vascular smooth muscle cells and collagen as an arterial media mimic. After 7-day culture, EPCs, which migrated from the stent struts, proliferated and endothelialized the luminal surfaces of the hybrid vascular medial tissue. This in vitro pilot study prior to in vivo experiments suggests that on-stent cell delivery of EPCs may be novel therapeutic devices for re-endothelialization or endothelium lining or paving at an atherosclerotic arterial wall, resulting in the prevention of on-stent thrombus formation and in-stent restenosis, as well as the rapid formation of normal tissue architecture.

Keywords: Stent; Endothelial progenitor cell; Re-endothelialization; Atherosclerosis

1. Introduction

An angioplastic procedure using a metallic stent is a standard of percutaneous therapy of coronary artery disease. However, the coronary stent implantation provokes a cascade of cellular and biochemical events that induce pathophysiologic process such as thrombus formation and release of cytokines which trigger the proliferation of smooth muscle cells (SMCs). Thus, the occurrence of sudden occlusion due to on-stent thrombus formation in the early period [1] and in-stent restenosis in the later period [2] after stent deployment is the principal drawback of coronary angioplasty. If rapid re-endothelialization, which provides an inherent nonthrombogenic potential and interrupts cytokine-driven activation of SMCs in vascular medial tissues, is achieved, accelerated normal wound healing at diseased sites may be realized. To this end, an intraluminal delivery of a sufficient number of endothelial cells (ECs) to diseased arterial sites is a promising approach.

Previous animal studies revealed that an enhanced re-endothelialization and inhibition of neointimal hyperplasia can be realized by EC seeding [3–5]. The cell delivery from a specially designed catheter may be a less effective method than on-stent cell delivery because of a very short period (less than a few minutes) of cell infusion for the catheter-based delivery and of delamination due to reperfusion, which may detach cells that are not fully adhered [6]. Experimental attempts of using EC-seeded stent struts were reported [7–9]. Irrespective of whether an on-stent or catheter-infusion delivery system is used, however, difficulty of harvesting EC from patients with atherosclerotic diseases has hampered clinical usage of these methods.

In this article, the authors address the fabrication procedures of cell delivery-stent devices of endothelial

*Corresponding author. Tel.: +81-92-642-6210; fax: +81-92-642-6212.
E-mail address: matsuda@med.kyushu-u.ac.jp (T. Matsuda).

0142-9612/03/$ - see front matter © 2003 Elsevier Science Ltd. All rights reserved.
doi:10.1016/S0142-9612(03)00042-5

progenitor cells (EPCs) seeded using either the surface of a stent strut or the surface of a covered stent to promote rapid re-endothelialization and the in vitro experimental model for re-endothelialization.

2. Methods

2.1. Canine endothelial progenitor cell (EPC) culture

The protocol for the care and use of animals was conducted according to the revised protocol of the Committee of the Ethics on Animal Experiment at the Faculty of Medicine, Kyushu University and the control of the Guideline for Animal Experiment at the Faculty of Medicine, Kyushu University and Law no. 105 and Notification no. 6 of the Japanese Government. The detailed procedure of harvesting and clonal growth of canine EPCs was reported previously [10]. Briefly, the mononuclear cells of the peripheral blood (15 ml) of an adult mongrel dog was collected by the gradient density centrifugation technique, and cultured on a type-I collagen-coated dish in EC basal medium 2 (Clonetics, San Diego, CA) supplemented with 20% fetal bovine serum (FBS, Life Technologies Inc., Rockville, MD) and 0.94% EGM-2 MV (Clonetics, San Diego, CA) containing vascular endothelial growth factor (VEGF). The details of the procedures were reported previously [11].

2.2. Fabrication of EPC-seeded devices

Photocured gelatin-coated stents were prepared (Fig. 1) according to our previously reported method [12]. Briefly, an aqueous solution of photoreactive gelatin (mol. wt. 9.5×10^4 g/mol; 20 mg/ml), which was partially derivatized with benzophenone group (12.5 benzophenone groups per gelatin molecule) which produces photoinduced radicals upon ultraviolet (UV) irradiation, was dip-coated on experimental gold stents (diameter 1.5 mm, length 20 mm, prototype stents supplied by Odensha Co., Ltd., Kawasaki, Japan) by immersion into the solution. The stents were subsequently irradiated with UV light for 10 min using a UV light source (Photocure 200, Hamamatsu Photonics Inc., Hamamatsu, Japan). These coating procedures were repeated two times. The gelatin-coated stent was placed into a six-well cell culture dish (Corning Inc., Corning, NY), and 1 ml of EPC-containing medium (1×10^6 cells/ml) was added in the well. After 1 h of incubation, another cell suspension was added in the same manner after the stent was rotated approximately 120° around its longitudinal axis. After repeating this procedure three times, the stent was incubated for 7 days.

Multiply micropored elastomeric film-wrapped stent and its photocured gelatin coating were fabricated according to our previously reported method [12,13]. Briefly, a piece of segmented polyurethane (SPU) film (thickness: 50 μm, Sheedom Co., Ltd., Tokyo, Japan) was multiply micropored (pore-to-pore distance: 1 mm, pore size: 150 μm) using a carbon dioxide laser cutting apparatus controlled through a personal computer via a computer-assisted design software (AutoCAD LT, Autodesk, Tokyo, Japan). The microporous SPU film cut to 21 mm × 6 mm was rolled around the stent and glued (Fig. 5A) using DMF (*N,N*-dimethylformamide), and subsequently coated with photoreactive gelatin aqueous solution (100 mg/ml) four times, as mentioned above. EPCs were seeded onto this microporous thin

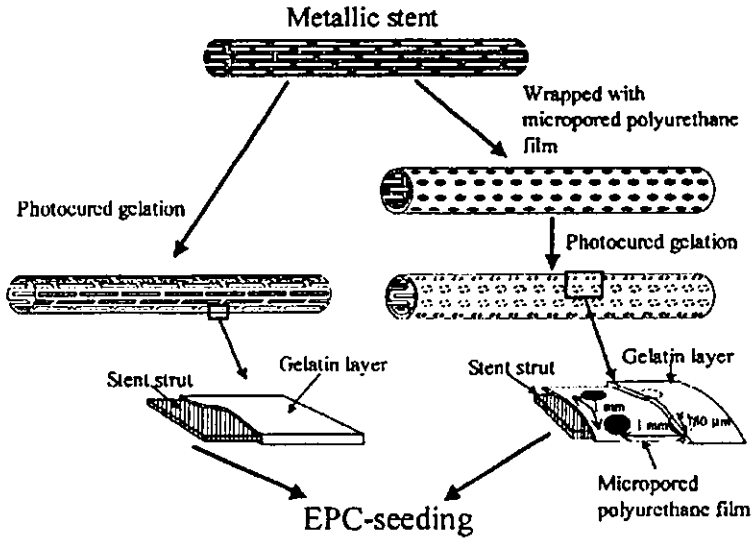

Fig. 1. Fabrication procedures of EPC-seeded devices. Experimental gold stent and multiply micropored elastomeric film-wrapped stent were coated and photocured with photoreactive gelatin. EPCs were seeded onto those stent devices.

SPU-covered stent in the same manner as the direct seeding of EPCs onto the photocured gelatin-coated stent.

These devices were loaded on the balloon site of a Multi-Link catheter (3.0 mm inflated diameter; Advanced Cardiovascular Systems, Hampshire, UK) and the balloon was inflated to expand those fabricated devices (inflation pressure; 10 atm, duration; 60 s, Figs. 3A and B).

2.3. Fabrication of hybrid vascular medial tissue

A tubular hybrid medial tissue used for in vitro examination was fabricated according to the method previously reported [14]. Briefly, a cold mixture of canine SMC suspension (8×10^6 cells/ml, 8 ml) in M199 supplemented with 10% FBS and 8 ml of acid solubilized bovine dermal type-1 collagen solution (3 mg/ml) was filled in the space between the sheath (inner diameter: 15 mm) and the mandrel (outer diameter: 3 mm) of a tubular glass mold. After incubation at 37°C for 30 min, the outer sheath was removed, and the resultant gel was incubated for 7 days to form a densely compacted tubular hybrid medial tissue.

2.4. In vitro stent implantation

Fluorescence-labeled EPCs (DiO, Vybrant DiO Cell-Labeling Solutions; Molecular Probes Inc., Eugene, OR), which were prepared according to the manufacturer's instructions, were used for loading EPCs onto stents so that implanted EPCs could be distinguished from SMCs in the hybrid vascular medial tissue. The EPC-seeded stent was attached to the catheter and inserted into the hybrid vascular medial tissue and the balloon was inflated with a manual inflation device (inflation pressure: 10 atm, duration: approximately 30 s). The hybrid-vascular-medial-tissue-implanted EPC-seeded stent was incubated for 7 days.

2.5. Histological study

The von Willebrand factor (vWF), Flk-1 (VEGF receptor-2), and acetylated LDL were used as endothelial markers. Second-passage EPCs were stained with primary antibodies [rabbit anti-human vWF polyclonal antibody (Dako Corp., Carpinteria, CA) and mouse IgG against human Flk-1 (Santa Cruz Biotechnology Inc., Santa Cruz, CA)]. Reactions were visualized by using peroxidase-conjugated secondary antibodies [EnVision + Peroxidase Rabbit and Mouse (Dako Corp., Carpinteria, CA)] and 3,3′-diamino-benzidine-tetrahydrochloride (Merck, Darmstadt, Germany). Acetylated LDL uptake by second-passage EPCs was examined in a medium containing 20 μl/ml DiI-acetylated-LDL (Biomedical Technologies Inc., Stoughton, MA) for 4 h at 37°C.

EPC-seeded devices were fixed and nuclei of the seeded cells on the devices were stained with Picogreen ds DNA Quantitation Reagent (Molecular Probes Inc., Eugene, OR) and examined by confocal laser-scanning microscopy (CLSM, Radiance 2000, Bio-Rad Laboratories Inc., Hercules, CA). Scanning electron microscopy (SEM, JSM 840A, JEOL Ltd., Tokyo, Japan) observation was also performed for the EPC-seeded stent. To evaluate the luminal surface of the hybrid-vascular-medial-tissue-implanted EPC-seeded stent, the DiO-labeled cell area was examined by CLSM.

3. Results

Canine EPC culture in the VEGF-containing medium on type-1 collagen-coated dishes resulted in the development of colonies of proliferative EPCs, which appeared at approximately 10 days after plating, and subsequent subculture resulted in exponential growth to produce 1.5×10^8 cells within 2 months after venipuncture. Immunohistochemical staining for endothelial markers of second-passage EPCs showed that almost all of the cells (> 98%) were positively stained with the

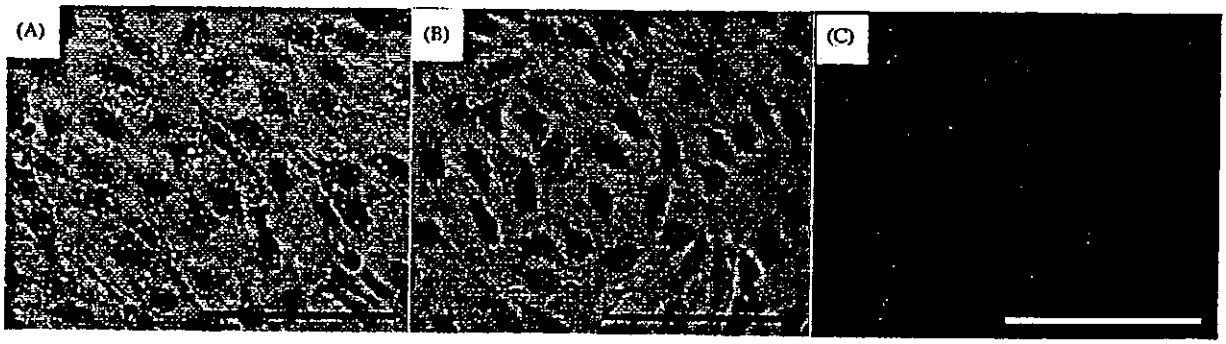

Fig. 2. Light micrographs of EPCs stained positively for vWF (A) and for Flk-1 (B). (C) CLSM image of EPCs taking up DiI-acetylated-LDL. Original magnification × 400, Bar = 100 μm.

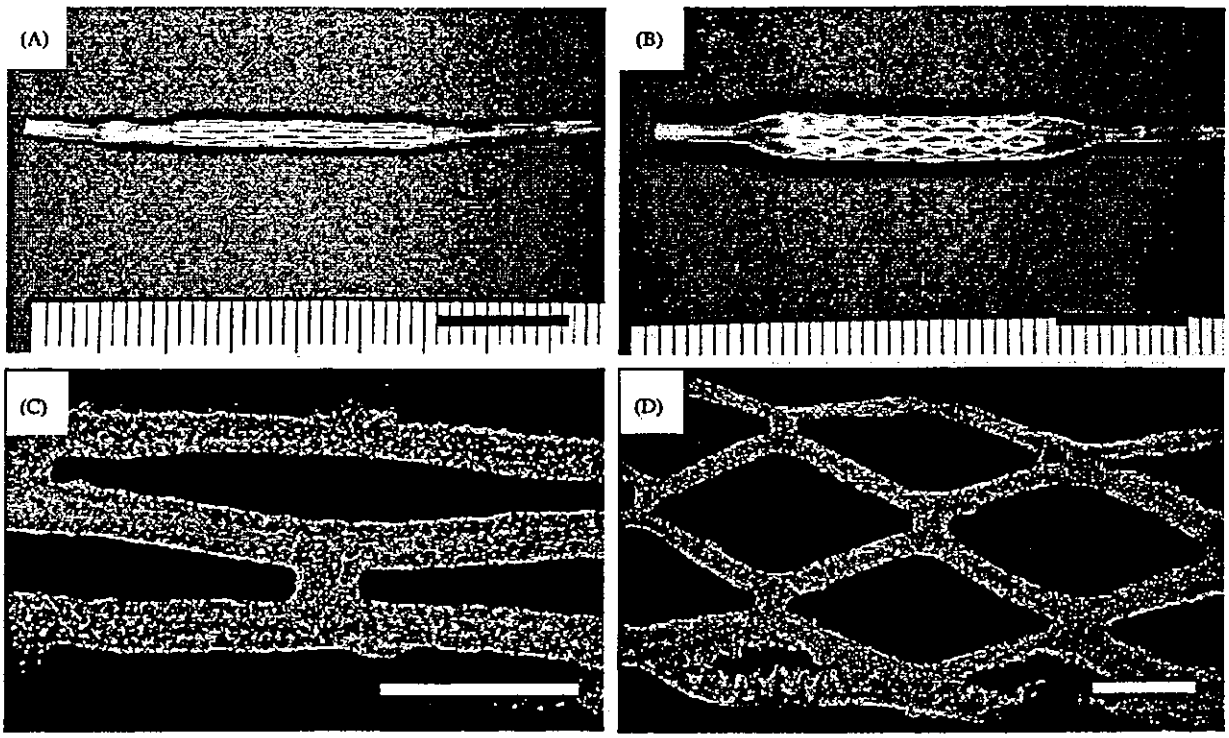

Fig. 3. EPC-seeded stent. EPC-seeded stent was attached to a balloon catheter (A), and expanded by balloon inflation ((B), outer diameter of inflated balloon: 3 mm). (C) CLSM image of EPC-seeded stent. Nuclei of EPCs were stained with Picogreen (green fluorescence). Original magnification × 40, Bar = 1 mm. (D) CLSM image of EPC-seeded stent after balloon expansion. Original magnification × 20, Bar = 1 mm.

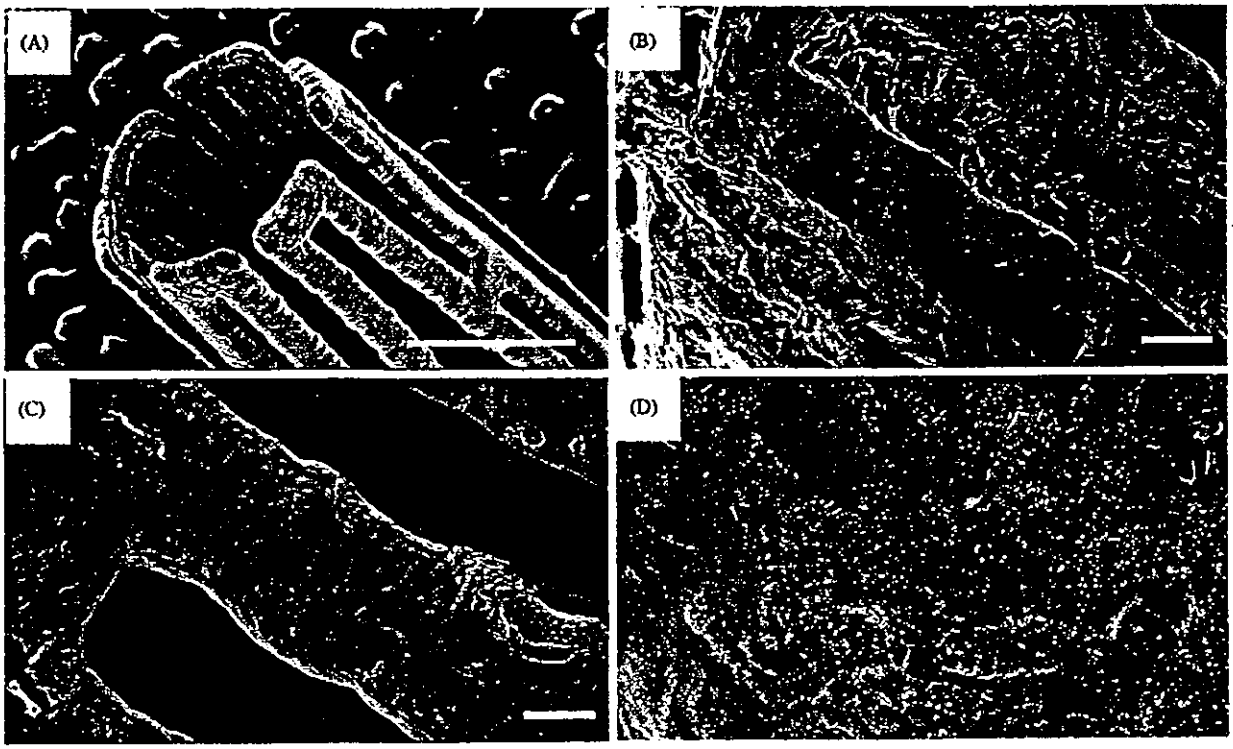

Fig. 4. SEM photographs of EPC-seeded stent. (A) Outer surface of the stent (original magnification × 35, bar = 1 mm). (B) Luminal surface of the stent (original magnification × 150, bar = 100 μm). (C), (D) High magnified micrographs of the stent. Stent struts were fully covered by confluent monolayer of EPCs ((C), original magnification × 150, bar = 100 μm). The EPC layer showed cobblestone appearance ((D), original magnification × 800, bar = 10 μm).

vWF antibody and Flk-1 antibodies (Figs. 2A and B). Fluorescent micrographs showed that EPCs also took up DiI-Ac-LDL (Fig. 2C).

Two types of tissue-engineered stent (EPC-seeded stent and EPC-seeded covered stent) were examined before and after stent expansion. CLSM examination showed that the surface of EPC-seeded stent was almost fully covered with Picogreen stained EPCs-monolayer (Fig. 3C). SEM examination showed that EPCs constructed cobblestone-like cell layer on the stent struts and the cell layer surrounded the whole struts uniformly (Fig. 4). After balloon expansion, in which an EPC-seeded stent was installed, the entire confluent cell layer was maintained on stent struts (Fig. 3D). The EPC-seeded covered stent was also covered completely with seeded EPCs (Fig. 5B). After stent expansion, the covered stent retained its cell-covered surface except at micropores, and cells located near the micropores were elongated in the direction of expansion (Fig. 5C).

To examine whether EPC migration from stents and proliferation to form a new endothelium on the luminal surface of hybrid vascular medial tissue occur, the EPC-seeded stent was expanded in the medial tissue (Figs. 6A and B). After 7 days of incubation in the hybrid medial tissue, CLSM analysis showed that the luminal surface of hybrid medial tissue was fully covered with DiO-labeled EPCs except where stent struts were attached. The luminal surface of implanted stent struts was also fully covered with DiO-labeled EPCs (Fig. 6C).

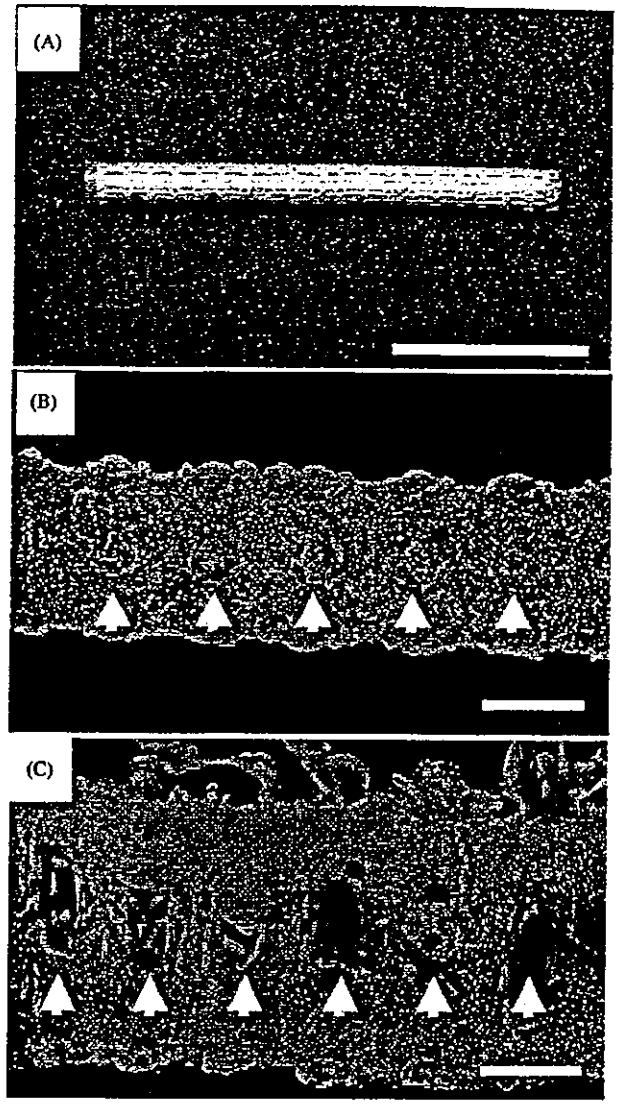

Fig. 5. (A) Gross apparatus of microporous thin polyurethane-covered stent. Bar = 10 mm. (B) CLSM image of EPC-polyurethane hybrid covered stent. Nuclei of EPCs were stained with Picogreen. Arrowheads indicate micropores. Original magnification × 20, Bar = 1 mm. (C) CLSM image of hybrid EPC-polyurethane covered stent after balloon expansion. Arrowheads indicate micropores. Original magnification × 20, Bar = 1 mm.

4. Discussion

Deployment of intravascular stents in humans is complicated by local thrombus which is induced by endothelial denudation [15] and/or injury occurring after angioplasty or caused by the surface of stent struts. Injured arterial walls, which lose their intact endothelium [16,17] or undergo foreign body reaction on the stent struts, become susceptible to local thrombus formation, which induces phenotypic alteration (from contractile to synthetic phenotype) of vascular SMCs due to potent mitogenic cytokine, platelet-derived growth factor secreted from platelets in the thrombus [18,19]. The stimulated SMCs migrate into and proliferate in intima and produce a large amount of extracellular matrices. These sequential molecular and cellular events eventually result in neointimal hyperplasia [20]. To solve these problems associated with intravascular stenting, enhancement of rapid re-endothelialization, re-endothelium-paving or relining at denudated regions has been proposed and attempted using a number of techniques [3–5,21–24]. In particular, seeding of stents with autologous EC is an attractive strategy for the prevention of stent-related thrombi without adverse side effects, and previous reports indicated that EC seeding reduces the area of neointimal hyperplasia [3–5].

Genetically engineered EC-seeded stents by which high local concentrations of therapeutic agents such as angiogenic, vasoactive, and antineoplastic peptides can be delivered to specific vascular beds are expected to be achieved. If they are properly seeded with a sufficient number of ECs, minimal loss of cells due to balloon trauma and flow effects after balloon expansion should be realized.

However, such EC-seeding methods have not resulted in extensive utilization in humans because of the